

TIME-AVERAGED PHENOMENOLOGICAL INVESTIGATION OF A WAKE BEHIND A BLUFF BODY

G.M.R. Van Raemdonck* and M.J.L. van Tooren†

*Design Integration and Operations of Aircraft and Rotorcraft
TU Delft, Faculty of Aerospace Engineering, Kluyverweg 1, 2628HS Delft, The Netherlands
e-mail: g.m.r.vanraemdonck@tudelft.nl

†Design Integration and Operations of Aircraft and Rotorcraft
TU Delft, Faculty of Aerospace Engineering, Kluyverweg 1, 2628HS Delft, The Netherlands
e-mail: m.j.l.vantooren@tudelft.nl

Keywords: Time-Averaged, Bluff Bodies, Experimental Research

Abstract: Drag reduction of road transport vehicles is a societal need that justifies increased interest in bluff body flows. The suggestion of Hoerner et al that thin boundary layers lower the pressure at the back of bluff bodies has been the inspiration for an experimental campaign to study the relation between boundary layer thickness and back pressure. By varying forebody roughness on a bluff body a coupled and controlled change in drag, base pressures, the thickness of the boundary layers and the structure of the wake has been obtained. A generalized representation of a European tractor-trailer combination was designed and made as wind tunnel model, called GETS. The results presented here are a time-avered analysis and show a strong interaction between the boundary layers, the drag and the pressures at the back.

1 INTRODUCTION

Background. Rising fuel prices force road transport companies to cut cost in order to stay competitive. The expected significant road transport demand in the next twenty years and the increasing environmental constraints has renewed the interest in truck design; any reduction in truck fuel consumption can be associated with large annual fuel cost reduction and considerable emission savings. Trucks can be seen as complex versions of blunt based bluff bodies.

The main aerodynamic features which are characteristic for a blunt based bluff body are the large region of separated and recirculating flow behind the body, a large pressure drag and highly unstable wake. The abrupt geometrical change at the base of the bluff body leads to flow separation and the formation of a dead air region. It is the low base pressure within the wake that is mainly responsible for the pressure drag of bluff bodies.

The flow contained within the region of the wake is dominated by the formation of large and small vortices combined with locally large amplitude velocity fluctuations in the wake. These fluctuations frequently occur associated with the shedding of vortices. For two dimensional bodies the near wake is dominated by the periodic and alternate shedding of vortices known as the Von Kármán vortex street. The most well researched body to show this phenomenon is that of the circular cylinder and a summary of the knowledge that has been accumulated over the years is given by Roshko [29].

For flows around symmetric and fully three dimensional bodies, however, wake periodicity is found to be a much less prominent feature. The flow around these types of bodies is extremely complex because vorticity shed from the body has components in all three directions.

Another aspect which adds to the complexity of these flows when considering road vehicles is the effect that is induced by the presence of the ground. A vehicle body within close proximity of the ground induces a boundary layer on the ground floor. This boundary layers has influence on the drag levels, the back pressures and the structure of the wake.

Past research on flow phenomenons of bluff bodies. The unsteady wake of a blunt based road vehicle was investigated by Duell and George [13]. In their work they hypothesized that the wake is dominated by the pumping effect of the wake behind the bluff body. Duell and George observed that a large ring-type vortex is present within the the recirculation region between the bluff body base and the free stagnation point of the wake. They suggested that this free stagnation point is in fact a quasi-periodically fluctuating point that shifts as vortices are shed from the shear layer to which Duell and George are referring to as the pumping effect.

Other experimental research concerning the bubble pumping theory are from Khaligini [20], Bayraktar [5] and the thesis of Balkanyi [2]. With the aid of the Large Eddy Simulation (LES) together with the increasing computer power, Krajnovic and Davidson ([21], [22], [23], [24] and [25]) were able to improve the insight in the different flow mechanisms around bluff bodies. Their studies with LES [22] have shown that the instantaneous flow is very different from the time-averaged one, not only in the wake but also along the entire body.

Basford [4] and Hoerner [18] suggested, that a thin boundary layer at the side of a bluff body is responsible for more negative pressure in the wake than a thick boundary layer. Or in other words a properly rounded front, responsible for the thin boundary layer and a lower drag coefficient, has as consequence lower pressures at the back of trailer, while a front with sharp corners and thus thicker boundary layers along the body results in higher back pressure coefficients.

Balkanyi [2, 3] gives the following interpretation. The abrupt geometrical change at the base of the bluff body leads to flow separation and the formation of a dead air region which results in the formation of a free shear layer. Through this shear layer, mass is entrained from the dead air region, which results in low pressure at the base of the model and an upstream flow at the center of the dead air region. Entrainment also causes the shear layer to grow and eventually merge with the shear layers formed on the other sides of the model. The same principle of mass entrainment and return between the shear region and the recirculation region is stated by Maull [26] for two dimensional bluff bodies.

Present research. For two dimensional profiles the wake and its size is a measure for the total drag which includes the friction and the pressure drag of that profile. But, is this still the case for bluff bodies with a blunt base? The goal of this research is to define a relation between different boundary layer thicknesses, the total drag of the corresponding body, the pressures at the back surface and the size of its wake. This relation should provide more insight in the flow behavior around and in the wake of bluff bodies. The suggestion by Hoerner et al will be verified.

Therefore an experimental phenomenological research of the flow in two different phases, of which the first phase is presented here, is being executed with a bluff body. The bluff body used represents a European tractor-trailer combination. Five different forebody roughness's are added which induces different boundary layers thicknesses. Performing time-averaged force measurements and pressure measurements, boundary layers thickness and planar PIV (Particle Image Velocimetry) measurements will contribute to define a mutual relation and to a better understanding of the behavior of the flow past the bluff body.

In a second phase time-dependent pressure at the surfaces and velocity field measurements (spectral analysis) together with more advanced PIV (stereoscopic and high speed) will be executed. Extensive three dimensional numerical simulations will help with the preparation of these wind tunnel tests.

2 EXPERIMENTAL SET-UP

2.1 Wind tunnel model

A new wind tunnel model was designed that meets the different requirements in order to perform the desired research and is based on a European tractor-trailer combination used for international road transport, illustrated in fig.1. The new wind tunnel model is symmetrical in the vertical and the horizontal plan, is made according to the maximum dimensions of a European tractor-trailer combination (length=16.5m; width=2.6m; height=4m; [15]), induces proper turbulent boundary layers, equipped with several pressure orifices, suitable to execute oil visualization and other measuring techniques like for instance PIV. Also the guide lines of the Society of Automotive Engineers concerning wind tunnel testing of bluff bodies SAE J1252 [30] are considered with respect to Reynolds number and blockage effects.

This SAE J1252 standard guide line defines: (1) the frontal area A at zero yaw angle should not exceed 5% of the active test section area C (the area above the ground board); (2) the model height should not exceed 0.3 of the test section height; (3) the projected frontal width when yawed to the maximum angle required should not exceed 0.3 of the tunnel width; (4) the mini-

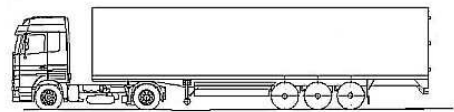


Figure 1: Tractor-trailer combination

mum acceptable test Reynolds number, based on the width of the model, is 0.7×10^6 . In terms of practicality the model may not be too long with respect to the measuring section of the wind tunnel to enable access to the wake of the body and to get the desired location of the model on the ground board: the ground board should extend at least two body widths upstream of the model and four to six body widths downstream, [30]. After analysing the several requirements the dimensions of the new model were defined as shown in table 2. The main parameter to focus on was the length of the model, because it defines the space left on the ground board to conduct PIV measurements. A length of 1100mm was chosen for the wind tunnel model.

Figure 2: Wind tunnel model dimensions

length [mm]	1100
width [mm]	173
height [mm]	234
ground clearance [mm]	33
scale	1:15
A/C	0.02
ratio width model-section	0.22
ratio height model-section	0.24
test velocity V_t [m/s]	60
Reynolds number, \sqrt{A}	0.8264×10^6

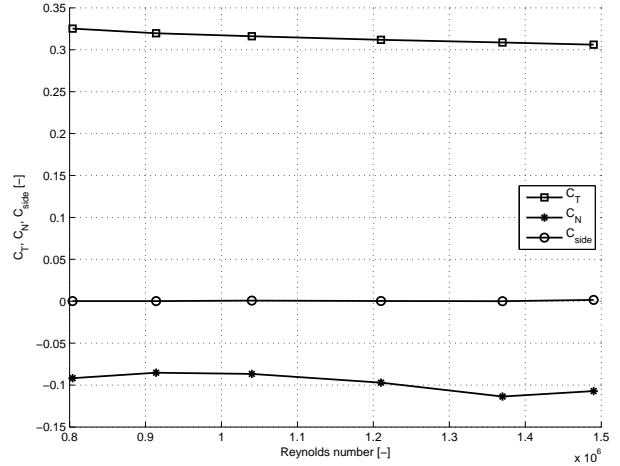


Figure 3: Reynolds effects

The Reynolds number for a European full-scaled truck, based on the square root of the frontal area of $A = 10.34m^2$, a driving velocity of $25m/s$, air density of $1.225kg/m^3$ and an air viscosity of $1.7894 \times 10^{-5}kg/ms$, becomes 5.5×10^6 [10]. By defining the general dimensions of the wind tunnel model the Reynolds number, which is based on the square root of the frontal area, could be calculated by selecting a test velocity. It turned out that $60m/s$ gives a Reynolds number of 0.8264×10^6 that meets the requirements set by SAE J1252 [30] for bluff bodies.

Front edge separation is an important aspect with truck aerodynamics and defines partially the drag coefficient of these vehicle. Front edge separation is undesirable within this research, therefore several radius ratios based on the width of the body and the frontal radius are recommended. Hoerner [18] defined a radius ratio of at least 0.1, while Hucho [19] proposes a ratio of at least 0.04. Within the experiments of Cooper [12] and Henneman [17] research is executed on front edge separation of truck like models within a certain range of radius ratios. Their experiments showed that a certain transcritical Reynolds number, $(Re_r)_t$, based on the radius of the frontal edge has a constant value of 1.24×10^5 for the turbulence intensity occurring in the wind tunnel test section. This transcritical Reynolds number can be defined as

$$(Re_r)_t = \frac{\rho r V_t}{\mu} \quad (1)$$

where ρ is the air density, μ the air viscosity, V_t the test velocity and r resembles the radius of the frontal edge. In order to calculate the radius of the frontal edges with the above eq.1, V_t is set on $50m/s$ to increase the velocity range where the boundary layer stays attached. This gives a radius of $36mm$ for all the frontal edges. This new wind tunnel model with the dimensions

of fig.2 and a frontal radius of 36mm is called GETS, Generalized European Transport System shown in fig.4, towards analogy with the NASA GTS experiments performed by Storms [31]. The GETS model is build-up with aluminum plates in a modular way to increase the flexibility towards other configurations and to create internal space for the pressure scanners.

The GETS model is tested within a velocity range of $50m/s - 100m/s$ in order to detect possible Reynolds effects. As fig.3 illustrates no global Reynolds effects were detected within the velocity range. However, care should be taken with the final settings of the test velocity due to small velocity differentiations and its influence on the different characteristics to be investigated.

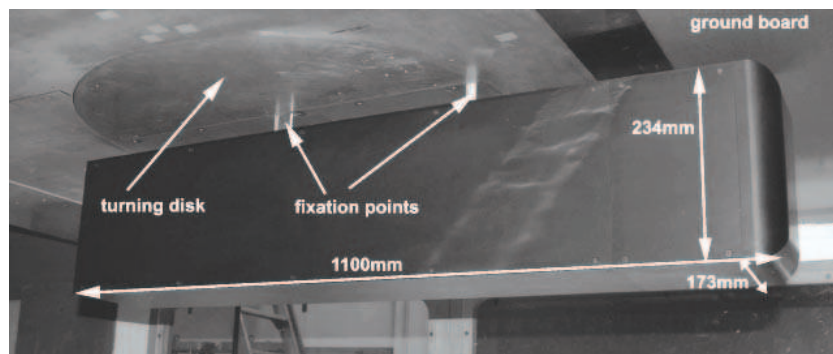


Figure 4: GETS model

In order to check if the rounded front edges of the GETS induces turbulent attached boundary layers two different methods were used. First, with a microphone one can detect if the flow is laminar or turbulent and if the boundary layer is attached or not. The microphone gave us the indication that the boundary layer was attached and turbulent just behind the rounded frontal edges. Secondly, oil visualization with parafine show the flow patterns and possible separation bubbles. Fig.5 illustrates just behind the front radius a collection (illuminated) oil: the flow is standing still which indicates the occurrence of a small separation bubble. This separation bubble can be avoided by adding zigzag-tape that triggers the boundary layers. As can be seen in fig.6, the separation bubble disappeared after adding zig-zag tape with a thickness of 0.65mm just in front the start of the start of curvature.

2.2 Wind tunnel configuration

The wind tunnel experiments were executed in the atmospheric Low Turbulence Tunnel (LTT, fig.7) of the Faculty of Aerospace Engineering at the Delft University of Technology, The Netherlands. This closed circuit wind tunnel has an octagonal test section with a cross sectional area of $2.07m^2$ (width of 1.8m; height of 1.25m, fig.8) and with parallel wind tunnel walls. The maximum operating velocity of the wind tunnel is 120m/s; the turbulence intensity can be changed in the range 0.02-0.1%. The empty test section is calibrated for the wind velocity with the aid of a pitot tube by measuring the dynamic pressure in the centre of the test section and compare it with a static pressure difference between two locations in front of the test section. Buckley [8] concluded after performing aerodynamic tests on the road and in the wind tunnel that the non-simulation of wind turbulence in the wind tunnel tests appears to be a significant contributing factor to the source of disagreement between the wind tunnel and over the road

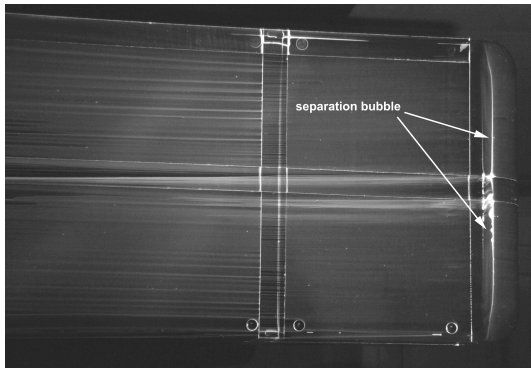


Figure 5: Flow visualization clean model

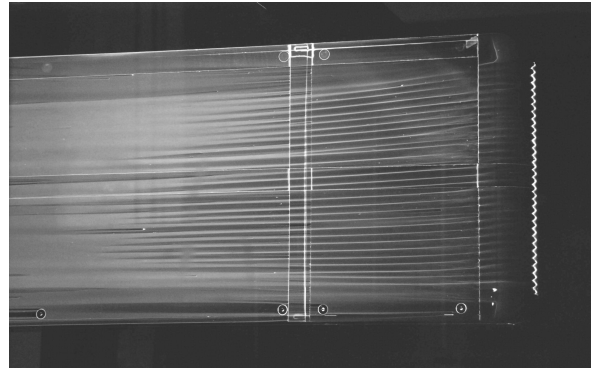


Figure 6: Flow visualization with 0.65mm thick zig-zag tape

drag reductions. On the road turbulence intensities of 10% and more were measured. Although the turbulence intensity of the flow has influences on its behavior there is decided to perform the tests with the maximum turbulence intensity of the LTT, which is 0.1%, and no further effort was put into artificially increasing the turbulence intensity.

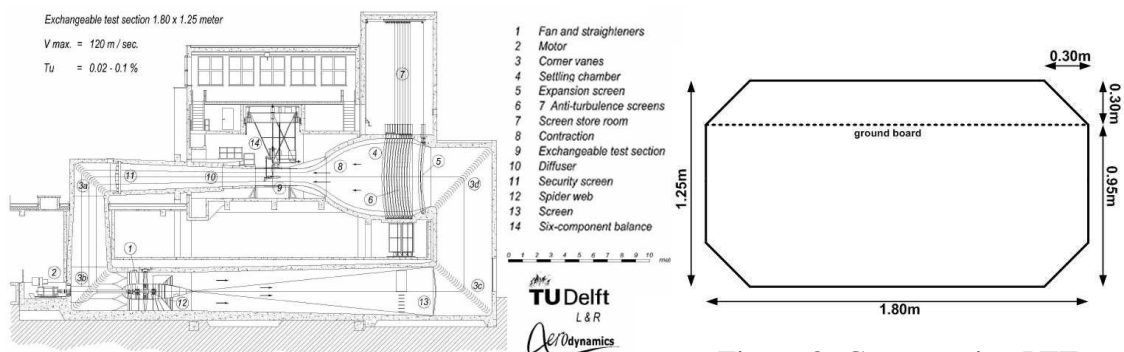


Figure 7: Low Turbulence Tunnel

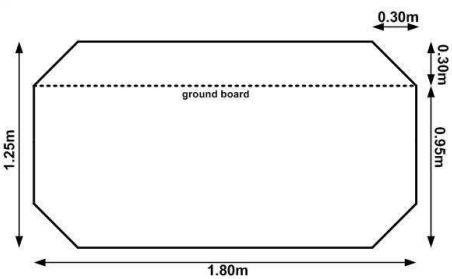


Figure 8: Cross section LTT

2.3 Ground effect

Due to the presence of a road vehicle a boundary layer is developing on the road itself. This boundary layer and thus the presence of a ground floor influences the boundary layer of the lower surface of the vehicle and its drag behavior. The wind tunnel used is not equipped with a moving belt which is desirable to investigate the ground effect of, for instance, race cars. Ground simulations and its study have been the subject of many research projects [7, 16, 27, 9, 14]. The most basic simulation approach used for passenger cars is the most direct and simple one: to test a vehicle on a fixed ground board. The major issue is a too thick approaching floor boundary layer. According to Cooper [10, 11] one can conclude that a fixed-floor with a thinned boundary layer is sufficient for current automotive and commercial vehicle applications, particularly where the underbody clearances are large.

To test the vehicle the model is suspended on a parallel floor (ground board) which has an offset of 300mm with respect to the upper (horizontal) wind tunnel wall and has the same width as the test section, fig.8. On the rounded front edge of this ground plate develops a new thinner boundary layer compared to the thick boundary layer on the wind tunnel wall.

2.4 Measuring techniques

Aerodynamic forces. The six-component mechanical balance system, located above the wind tunnel test section (see fig.7) measures the resulting aerodynamic forces acting on the GETS model. All the different force coefficients will be discussed: drag coefficient C_T , lift coefficient C_N and side force coefficient C_{side} . The direction of C_T is orientated in the longitudinal direction of the GETS model towards the back, the lift coefficient upwards and the side force coefficient perpendicular to the orientation of the drag coefficient. All the coefficients were averaged over 20 measuring points and calculated with the instant temperature in the settling chamber and the instant atmospheric pressure in the control room. The drag coefficient is not corrected due to blockage effects of the model.

Surface pressures. The pressure on the different surfaces is measured to calculate a corresponding pressure coefficient C_p . The back surface of the GETS model is equipped with 63 pressure orifices. The locations of these pressure orifices is illustrated in fig.9. The back pressures are measured with an Initium [32] pressure scanner with a range of 0-0.36psi. All the pressures were averaged in order to capture an average pressure field. No blockage correction methods were applied on the $C_{p,back}$.

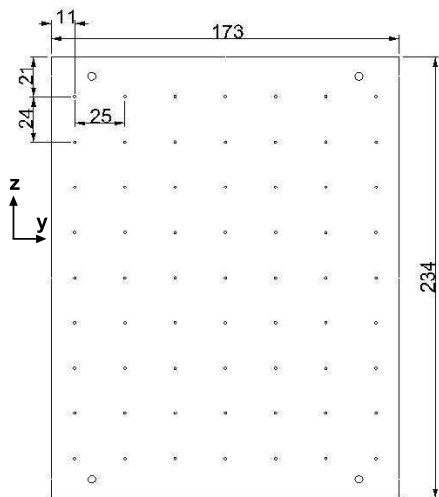


Figure 9: Pressure orifices on back surface

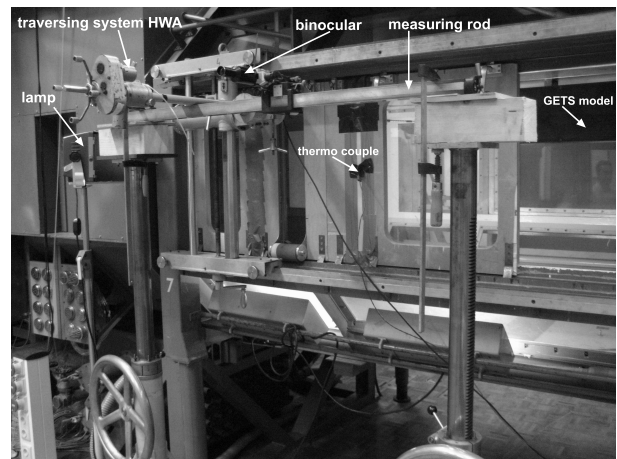


Figure 10: Experimental set-up hot wire anemometry

Boundary layer thickness. A single hot wire probe of DANTEC, probe type 55P11, mounted on a mechanical transverse system is used to measure the boundary layer thickness through measuring the velocity towards the model surface. The hotwire is calibrated in an empty test section. During the measurements the voltage signal is corrected for the temperature of the flow in the test section. The thickness of the boundary layer is measured in the middle and 15mm in front of the rear edge of the left side surface of the GETS model. A rather unusual measuring technique is applied in order not to break the hot wire when traversing towards the body surface. A strong lamp illuminates the hot wire probe. With a binocular, which can be slided parallel to the flow on a measuring rod, the hot wire itself and its shadow can be observed.

The distance between the hot wire and its shadow can be read from the measuring rod. If this mutual distance becomes zero, the hot wire touches the surface which should be avoided. This experimental set-up for the hot wire is illustrated in fig.10.

Wake structure. A Particle Image Velocimetry (PIV) system was used to measure the velocity field of the wake and to get insight in its structure. The main components of the PIV system were: a Quantel Twins CFR 200 PIV 200mJ laser of NdYAG, a LaVision Imager Intense high resolution camera and a SAFEX fog generator. The dual NdYAG laser was used to illuminate the flow, from underneath the wind tunnel test section, with the aid of small particles polluted by the fog generator. The output beams of the laser were directed into the test section by a set of mirrors and shaped into a light sheet with a width of 350mm and thickness of approximately 2mm. This light sheet was orientated in the direction of the flow and placed in the symmetry plane of the wake of the model. Inside the test section the wind tunnel walls were made black in order to minimize laser reflections and to increase the illumination effect of the laser. Hard- and software of Davis was used to perform the PIV measurements. The post processing of the images was done with an in-house developed Matlab routine.

3 EXPERIMENTAL RESULTS

The objective of the experiments is to find a correlation between the drag coefficient of the bluff body, the average pressure coefficient at the back surface, the thickness of the boundary layer and the structure of the wake. Let starts with discussing the several characteristics alone. During the experiments roughness is added at the frontal surface in terms of zig-zag tape to induce thicker boundary layers. Five different thicknesses were tested: 0mm (no zig-zag tape), 0.65mm, 1.05mm, 1.55mm and 2.05mm.

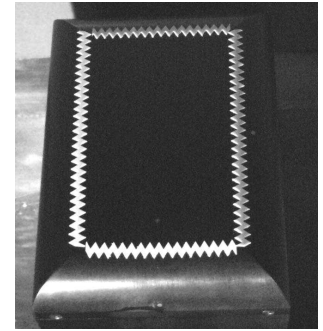


Figure 11: GETS with zig-zag tape

3.1 Aerodynamic forces

Fig.12 gives an overview of the different force coefficients with changing forebody roughness. As one can notice, the drag coefficient, fig.12(a) first drops from $C_T = 0.329$ (clean configuration) towards $C_T = 0.327$ for the 0.65mm thickness. The reason for this drop can be found in the fact that by adding zig-zag tape of 0.65mm the separation bubble disappears which gives a thinner boundary layer compared to the clean configuration. If the thickness of the zig-zag tape increases more, the drag coefficient becomes higher. The lift coefficient C_N is negative for all configura-

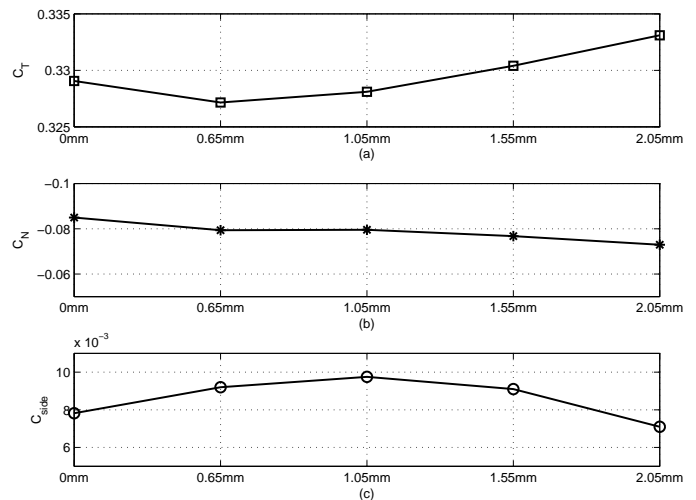


Figure 12: Overview of the different force coefficients C_T , C_N and C_{side}

tions, meaning that the GETS model is generating a downforce. This lift coefficient is mainly influenced by the presence of the ground floor and the corresponding boundary layers. Fig.12(b) shows a slightly decreasing lift coefficient due to the interference of the possible thicker boundary layer of the bottom surface of the model with the boundary layer of the ground board.

The side force coefficient C_{side} is very small and positive. A perfect symmetrical model should give a C_{side} of zero. The modular built up of the wind tunnel model gives small seams and the presence of (flat headed) bolts could be the reasons for these results. Therefore the seams and the bolts were filled up with clay as good as possible.

3.2 Pressures

The vertical cross section of the pressure field at the back surface of the GETS model in terms of pressure coefficient is shown in fig.13. The vertical axis of the figure resembles the relative height z/H of the model, the horizontal axis gives the average of the horizontal pressure coefficients at that height z/H . The figure indicates for the several pressure coefficient cross sections the expected S-curve: at the upper side of the back surface the strongest underpressures are occurring, while at the lower side of the back surface lower under pressures are present. Clearly noticeable in fig.13 is that the pressure coefficient of configuration 0.65mm close to the ground surface differs from the other configurations. This is also translated in fig.14 where one can observe the average pressure coefficient over the whole back surface. The configuration with the 0.65mm zig-zag tape has the lowest $C_{p,back}$ and thus the largest suction force on the back surface of the GETS model. After the $C_{p,back}$ drops from the clean configuration towards the 0.65mm configurations, it starts increasing again with increasing thickness.

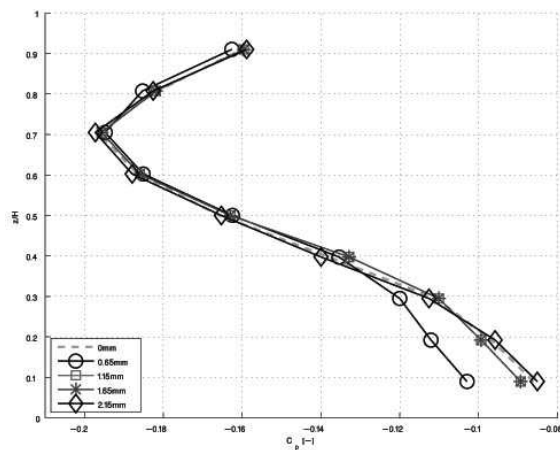


Figure 13: Overview of the pressure coefficients for the different configurations

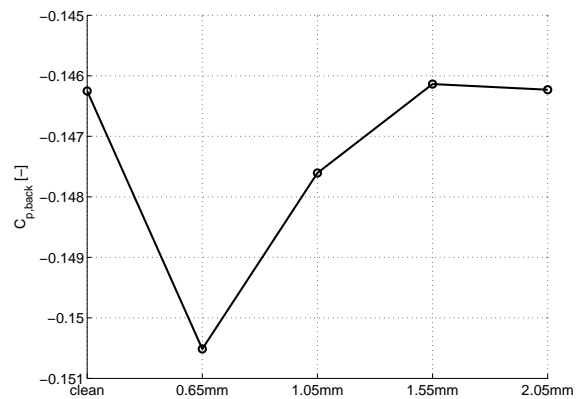


Figure 14: Overview of the average pressure coefficients for the different configurations

3.3 Boundary layer thickness

With the aid of a mechanical traversing system the velocity within the boundary layer is measured in several steps towards the surface of the GETS model with the hot wire. Close to the surface the measurements were stopped in order not to break the hot wire, at that moment the distance left towards the surface was estimated by measuring the distance between the hot wire probe and its shadow with the binocular mounted on the measuring rod. As mentioned before the voltage of the hot wire is being corrected for the flow temperature. Several boundary layer parameters were calculated: the displacement thickness δ^* , momentum thickness θ and shape factor H :

$$\delta^* = \int_0^\infty \left(1 - \frac{u}{U}\right) dy; \quad \theta = \int_0^\infty \frac{u}{U} \left(1 - \frac{u}{U}\right) dy; \quad H = \frac{\delta^*}{\theta} \quad (2)$$

The displacement thickness δ^* is the distance a streamline just outside the boundary layer is displaced away from the wall, while the momentum thickness is proportional to the decrement in momentum flow and gives an indication for the skin friction drag. The shape factor is often used in boundary layer analysis and gives information about the shape of the velocity profile: a small shape factor corresponds with a fuller velocity profile, while a large shape factor indicates a more unstable boundary layer that tends to separate from the surface.

Fig.15 gives the velocity profile together with the 3 different parameters for the configuration with the 0.65mm thick zig-zag tape. The displacement and the momentum thickness and the shape factor for a turbulent boundary layer on a flat plate with a length of 1100mm are, according to Anderson [1], respectively: 2.3655, 1.8513 and 1.2778. These theoretical values are close to the results obtained during the wind tunnel experiments. Fig.16 shows an overview of the boundary layer results with respect to the several configurations. As expected one can notice that the boundary layer thickness drops after adding the 0.65 zig-zag tape and increases again with the more thick tapes. Also the shape factor H changes which indicates a slightly more unstable boundary layer: the velocity profile changes towards an inflection point.

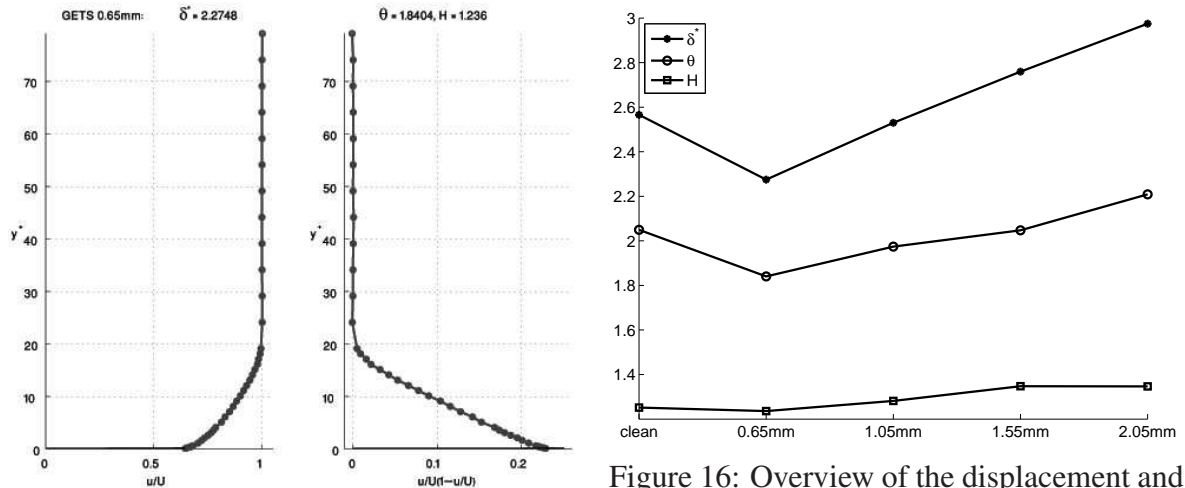


Figure 15: Velocity profile of the boundary layer of configuration 0.65mm

Figure 16: Overview of the displacement and momentum thickness and the shape factor for the different configurations

3.4 Wake structure

With the aid of PIV a 2 dimensional time-averaged velocity field of the wake in the symmetry plane of the model is being captured. This 2 dimensional wake can easily be characterized by the location of the free stagnation point (SP) that closes the wake and the locations of vortices. The location of this SP can be identified as follows: the horizontal distance L_{SP} and the vertical distance H_{SP} , see fig.17. Also in fig.17 the locations (height and length position) of the centre of the two counter rotating vortices v_1 and v_2 are indicated. These two counter rotating vortices are typical for a wake behind a bluff body: the upper vortex v_1 is stronger and bigger than the lower located vortex v_2 . The gray scale in fig.17 indicates the velocity component U m/s in x-direction of the vehicle. Clearly visible is the back flow in the middle of the wake.

Fig.18 gives an overview of the different locations of the SP and the centres of respectively vortex v_1 and v_2 . These results show that the SP moves in the z-direction according to the thickness of the zig-zag tape: the SP is at its lowest position for configuration 0mm, the position increases for configuration 0.65mm and decreases again. The x-direction of the stagnation point shows a rather different behavior: the SP moves more downstream with increasing thickness of the zig-zag tape, only for the last configuration the SP shifts upstream again. The location, in both directions x and z, of the largest vortex v_1 do not change significantly. Also the position of the second vortex v_2 stays rather constant only the x-position increases with increasing zigzag-tape thickness.

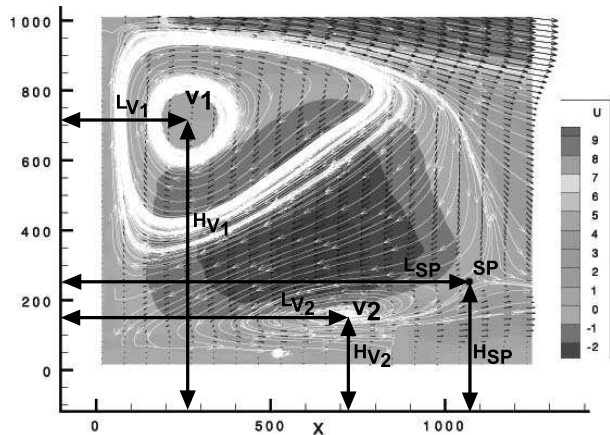


Figure 17: Wake structure of configuration 0.65mm

Figure 18: Wake structure parameters [pxl]

config.	H_{SP}	L_{SP}	H_{v_1}	L_{v_1}	H_{v_2}	L_{v_2}
0mm	238	1063	717	259	152	700
0.65mm	260	1068	713	263	155	709
1.05mm	257	1066	706	262	151	720
1.55mm	248	1087	706	263	150	724
2.05mm	241	1072	714	267	155	737

4 DISCUSSION WITH CONCLUSIONS

The clean configuration (without triggering the boundary layer) has the highest drag coefficient which can be expected due to the little separation bubble at the front edge, shown in fig.12(a). The configuration with the 0.65mm zig-zag tape indicated no separation bubbles, which results in the lowest C_T value. An increasing zigzag-tape thickness goes together with an increasing drag coefficient. The pressure coefficient at the back surface $C_{p,back}$, plotted in fig.14, has the same trend as the drag coefficient. It is remarkable, however, that at the lowest drag coefficient, the most negative pressure coefficient (highest suction at the back surface) is registered. And that for this particular configuration the most thin boundary layer is measured, see fig.16. The boundary layer thickness results have in general the same behavior as the drag

and pressure coefficients. In fig.19 the drag coefficient C_T and the time-average pressure coefficient $C_{p,back}$ of the back surface are plotted together with the variation of the displacements thickness δ^* which corresponds with the several configurations. The drag and the pressure coefficient have the same trend. The displacement thickness of the clean configuration lies close the δ^* of the 1.05mm configuration.

The statements earlier made in the introduction by Hoerner [18] are confirmed: a thin boundary layer gives a lower drag coefficient and a more negative pressure coefficient at the back. Adding roughness gives in certain situations a lower drag coefficient, higher underpressure at back surface and a less thick boundary layer; while in other cases the reverse happens: higher drag coefficient, less negative pressure coefficients and thick boundary layers.

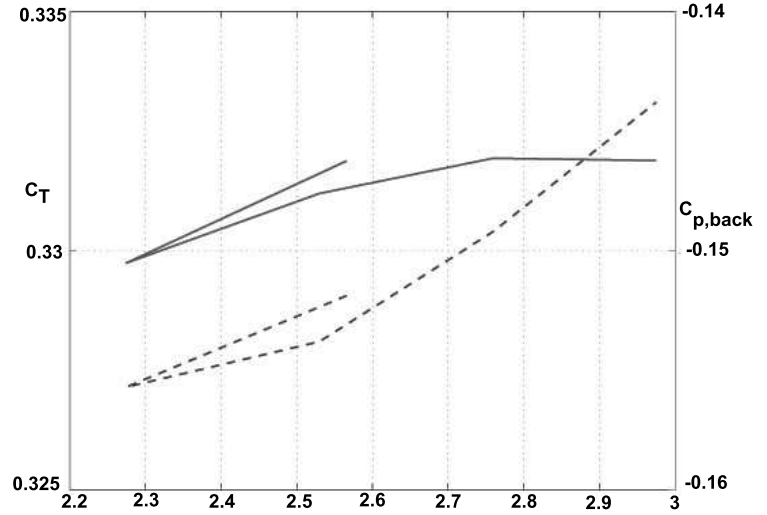


Figure 19: Drag together with pressure coefficients

The different x-positions of the stagnation point seems to show that with increasing drag coefficients the length of the wake increases while the vertical position of the SP decreases. The latter is probably due to the fact that centre of the second vortex v_2 is moving downstream, while the larger vortex v_1 keeps its positions. The boundary layer on the bottom surface of the GETS and its interaction with the ground board plays herein a crucial role. One has to keep in mind that these PIV measurements are 2D time-averaged representations of a wake that is dominated by 3 dimensional effects.

5 RECOMMENDATIONS

Time dependant measurements of the pressures and the velocity field, is necessary to make a next step towards increased knowledge of flow behavior around bluff bodies. A profound drag breakdown and analysis of the different drag contributions will contribute to the general understanding of bluff body flows. In addition yaw angle variation should be considered during this next phase, because the yaw angle has big influence on the structure of the wake, the drag levels and the occurring pressures.

To broaden the experimentally covered range of drag and pressure coefficients, boundary layer thicknesses and wake structures the model should allow for mounting of an extreme aerodynamically badly shaped frontal surface. A square front with sharp edges gives extreme values for these parameters and brings us to the edge of our range of interest.

The next step in flow visualization of the wake structure is using a high speed laser and high speed camera (several kHz) to capture the fluctuations within the velocity field of the wake and the fluctuations in the shear layers. With the aid of an electrical traversing system which can operate in all three directions a three dimensional image can be formed of the wake behind the body. Positioning of the model at the centre of the test section would cancel the influence of the ground board.

REFERENCES

- [1] Anderson, J.D., *Fundamentals of Aerodynamics*. McGraw-Hill International Edition, Second Edition, 1991.
- [2] Balkanyi, S., *An experimental investigation of drag reduction devices for blunt based road vehicles*. Master's thesis, Delft University of Technology, Faculty of Aerospace Engineering, 2001.
- [3] Balkanyi, S., Bernal, L., Khalighi, B., and Sumantran, V., *Dynamics of manipulated bluff body wakes*. AIAA Journal 2000-33888, 2000.
- [4] Basford, W., *Apparatus to reduce drag behind bluff bodies*, United States Patent 2002/0030384, 2002.
- [5] Bayraktar, I., Landman, D., and Baysal, O., *Experimental and computational investigations of Ahmed body for ground vehicle aerodynamics*. SAE Paper 2001-01-2742, 2001.
- [6] Bearman, P., *Some observations on road vehicles wakes*. SAE Paper 840301, 1984.
- [7] Berndtsson, A., Mason, W. E., and Mercker, E., *The effect of ground plane boundary layer control on automotive testing in a wind tunnel*. SAE Paper 880248, 1988.
- [8] Buckley, F.T.jr. Comparison of On-Road and Wind-Tunnel Tests for Tractor-Trailer Aerodynamic Devices, and Fuel Savings Predictions. SAE Paper 850286, 1985.
- [9] Carr, G., *A comparison of the ground-plane-suction and moving-belt ground-representation techniques*. SAE Paper 880249, 1988.
- [10] Cooper, K., *Bluff-body aerodynamics as applied to vehicles*. Journal of Wind Engineering and Industrial Aerodynamics, Vol.49, pp.1-21, 1993.
- [11] Cooper, K., *The wind tunnel testing of heavy duty trucks to reduce fuel consumption*. SAE Technical Paper 821285, 1982.
- [12] Cooper, K., *The Effect of Front-Edge Rounding and Rear-Edge Shaping on the Aerodynamic Drag of Bluff Vehicles in Ground Proximity*. SAE Technical Paper 850288, 1985.
- [13] Duell, E. and George, A., *Experimental study of a Ground vehicle body unsteady near wake*. SAE Paper 1999-01-0812, 1999.
- [14] Eckert, W., Singer, N., and Vagt, J.-D., *The Porsche wind tunnel floor-boundary-layer control - A comparison with road data and results from moving belt*. SAE Paper 920346, 1992.
- [15] FOCWA, rai, Transport en Logistiek Nederland, *Maten & Gewichten Editie 2002*. FOCWA en Transport en Logistiek Nederland, 2002.
- [16] Hacket, J., Baker, H., Williams, J., and Wallis, S., *On the influence of ground movements and wheel rotation in tests on modern car shapes*. SAE Paper 750245, 1975.
- [17] Henneman, B., *Modeling of Front Edge Flow Separation on Rounded Bluff Body Bodies Commercial CFD Software*, Master's thesis, Delft University of Technology, Faculty of Aerospace Engineering, 2005.
- [18] Hoerner, S., *Fluid-dynamic drag*. Hoerner Fluid Dynamics, Vancouver, 1965.
- [19] Hucho, W.-H., *Aerodynamics of road vehicles*, fourth edition, Hardbound, 1998.
- [20] Khalighi, B., Zhang, S., Koromilas, C., Balkanyi, S., Bernal, L., Iaccarino, G., and Moin, P., *Experimental and computational study of unsteady wake flow behind a bluff body with a drag reduction device*. SAE Paper 2001-01-1042, 2001.
- [21] Krajnovic, S. and Davidson, L., *Large-eddy simulation of the flow around a ground vehicle body*. SAE Paper 2001-01-0702, 2001.
- [22] Krajnovic, S. and Davidson, L., *Numerical study of the flow around a bus-shaped body*. Journal of Fluid Engineering, Vol. 125, 2003, pp. 500–509.
- [23] Krajnovic, S. and Davidson, L., *Large-eddy simulation of the flow around simplified car model*. SAE Paper 2004-01-0227, 2004.
- [24] Krajnovic, S. and Davidson, L., *Flow around a simplified car, Part1: Large Eddy Simulation*. Journal of Fluid Engineering, Vol. 127, 2005, pp. 907–918.
- [25] Krajnovic, S. and Davidson, L., *Flow around a simplified car, Part2: Understanding the flow*. Journal of Fluid Engineering, Vol. 127, 2005, pp. 919–928.
- [26] Maull, D., *Mechanism of two and three dimensional base drag*. Symposium on Aerodynamic drag mechanisms of bluff bodies and road vehicles proceedings, Plenum, New-York, September 1976, pp. 137-153.
- [27] Mercker, E. and Knape, H., *Ground simulation with moving belt and tangential blowing for full-scale automotive testing in a wind tunnel*. SAE Paper 890367, 1989.
- [28] Oertel, H.jr., *Wakes behind blunt bodies*. Annual Review of Fluid Mechanics, Vol. 22, 1990, pp. 539–564.
- [29] Roshko, A., *Perspectives on bluff body aerodynamics*, Journal of Wind Engineering and Industrial Aerodynamics, Vol. 49, 1993, pp. 79.
- [30] Society of Automotive Engineers, *SAE wind tunnel test procedure for truck and buses*. SAE J1252, 1981.
- [31] Storms, B.L. e.a., *An Experimental Study of the GTS Model in the NASA Ames 7-by 10-FT Wind Tunnel*. NASA/TM-2001-209621, 2001.
- [32] DTC Initium, http://www.pressuresystems.com/dtc_initium.html
- [33] Esterline Pressure Systems, http://www.pressure-systems.com/esp_scanners.html.